Journal of Sound and Vibration (2000) **233**(5), 813–833
doi:10.1006/jsvi.1999.2803, available online at http://www.idealibrary.com on IDEAL®

ELASTODYNAMIC RESPONSES OF AN IMMERSED COMPOSITE LAMINATE TO A GAUSSIAN BEAM PRESSURE

G. R. Liu, X. J. Wang and Z. C. Xi

Department of Mechanical and Production Engineering, National University of Singapore, 10 Kent Ridge Crescent, Singapore 119260, *Singapore*

(*Received* 10 *June* 1999, *and in final form* 22 *November* 1999)

An analytical method is presented for analyzing elastodynamic responses of an immersed composite laminate subjected to a Gaussian beam pressure. Firstly, the Fourier transform technique and a modal analysis method are combined to obtain the surface displacements in the frequency domain. Complex path techniques are proposed for dealing with singularities of the responses associated with the inverse Fourier transformation. A quadrature scheme is adopted to reduce the sampling points in the inverse Fourier transformation. Then elastodynamic responses of the laminate in the time domain can be found by application of Fourier superposition. An exponential window method is employed to overcome singularities of integrands at $\omega = 0$ and cut-off frequencies. The effects of the fluid on displacements in wave number, frequency and time domains are discussed. The presence of the fluid is found to have considerable impact on the responses of the composite laminate.

1. INTRODUCTION

The interaction of elastic waves with a fluid-loaded anisotropic laminate is frequently encountered in non-destructive evaluation of materials and underwater explosions. In these practical applications, the acoustic wave generated by a transducer or source of excitation propagates through the upper coupling fluid first and then onto the surface of the layered plate. This problem has received a large amount of attention in dynamics of advanced composite materials. Characterizing the wave propagation in a fluid–solid system, Mott [1] as well as Henneke and Jones [2] demonstrated theoretically and experimentally a lateral shift phenomenon of a reflected beam. Atalar [3] calculated reflection coefficients of sound waves incident on a liquid-cubic-crystal half-space. Arikan *et al.* [4] extended this investigation to a general anisotroic solid. Chimenti and Nayfeh [5] discussed the effect of solid material viscosity on reflection fields. Liu *et al.* [6] proposed a hybrid numerical method for studying elastic stress waves in a composite laminate subjected to a plane shock wave. Liu *et al.* [7] proposed an exact method and applied it to wave propagation in a composite laminate in contact with water on one side. Nayfeh [8] analyzed reflection coefficients from a fluid-monoclinic half-space. Nayfeh and Taylor [9] used a matrix transfer technique to obtain reflection and transmission coefficients for a fluid-loaded media. Qu *et al.* [10] studied reciprocity relations for waves propagating in a fluid-anisotropic half-space. Ann and Achenbach [11] calculated $\mathbf{V}(z)$ and $\mathbf{V}(x, z)$ curves for a line focus acoustic microscope and a specimen with a crack using the boundary element method. Liu *et al.* [12] combined the finite element method and the boundary element method to calculate $V(z)$ curves as well. They found that the attenuation of water

0022-460X/00/250813 + 21 $35.00/0

must be taken into account to get more accurate $V(z)$ curves. Mampaert *et al.* [13] used an analytical approach to study reflection and transmission of normally incident ultrasonic waves on periodic solid–liquid interfaces. Plona *et al.* [14] used experimental technique to examine the characteristics of wave propagation in an alternating fluid-plate layer system. Fay and Fortier [15] investigated wave transmission in immersed isotropic media. Nayfeh and Chimenti [16] studied experimentally wave reflection from an orthotropic plate immersed in a fluid. Based on an effective modulus theory, Dayal and Kinra [17] considered the propagation of leaky Lamb waves in an anisotroic plate. An exact solution for the dispersion equation was found. Furthermore, Dayal and Kinra [18] used non-destructive testing to investigate the matrix cracks in fiber-reinforced composites. Nayfeh and Chimenti [19] investigated elastic waves propagating in a fluid-loaded multiaxial anisotropic media via a transfer matrix method. Chimenti and Nayfeh [20] studied guided wave propagation in biaxially laminated composite plates. Nayfeh and Chimenti [21] conducted both theoretical and experimental investigations into reflection from a unidirectional fibrous composite plate immersed in water. They found that the Cremer correspondence principle was valid only when the ratio of fluid to solid density was small.

In this paper, an analytical method proposed in reference [7] is extended to compute the surface displacements of a composite laminate in contact with water on both sides, subjected to a Gaussian beam pressure. The formulation is also extended to the time domain. Detailed investigation is carried out into the effect of the fluid on the responses of the laminate in wave number, frequency and time domains. Firstly, the Fourier transform technique and a modal analysis method are combined to obtain the surface displacements in the frequency domain. Complex path techniques are proposed for dealing with singularities of the responses associated with the inverse Fourier transformation. A quadrature scheme is adopted to reduce the sampling point in the inverse Fourier transformation. Then the elastodynamic responses of the laminate in the time domain can be found by application of the Fourier superposition. An exponential window method is employed to overcome singularities of integrands at $\omega = 0$ and cut-off frequencies. In computations, the interaction between the laminate and water is taken into account. Numerical example are presented for a steel plate and a $[C90/G + 45/G - 45]_s$ composite laminated plate

2. PROBLEM STATEMENT

A composite laminated plate of thickness H and infinite length immersed completely in a fluid is shown in Figure 1. The plate is made of an arbitrary number of linearly elastic laminate. The bonding between plies is assumed to be perfect. Deformations of the plate are assumed to be small under the source of excitation. The Cartesian co-ordinate system is used. A transverse Gaussian beam applied at the upper water–plate interface is given as

$$F(x) = A \exp(-x^2/b^2)\exp(-\mathrm{i}\omega t), \tag{1}$$

where A is the amplitude of the Gaussian beam and b is the shape parameter, $\mathrm{i} = \sqrt{-1}$ and ω is the frequency. The Gaussian beam is a distributed load which approaches zero as $x \to +\infty$ or $x \to -\infty$; its amplitude coincides with the z-axis. Notice that for small b, the

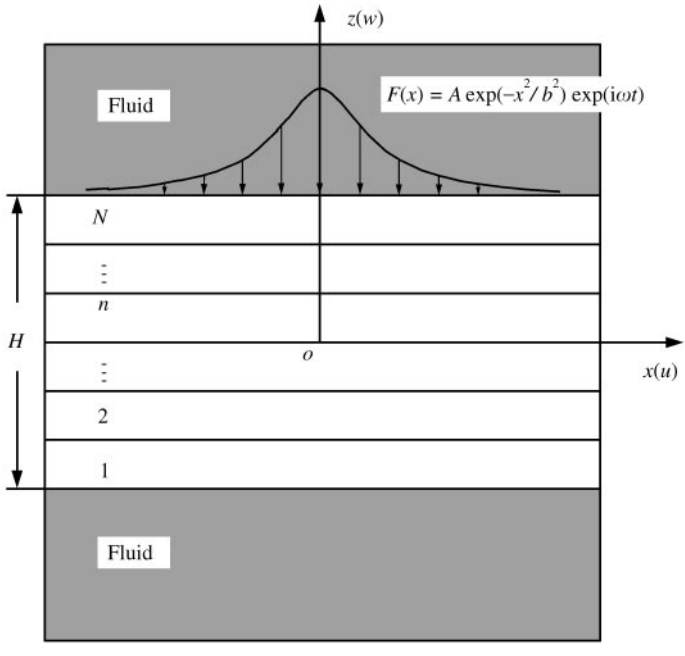

Figure 1. Geometry of an immersed composite laminated plate.

Gaussian beam is a concentrated load. In time domain, the wavelet is given as

$$F(t) = \begin{cases} \sin(2\pi t/t_d) & 0 < t < t_d, \\ 0, & t \leqslant 0,\ t \geqslant t_d \end{cases} \tag{2}$$

where t_d is the time duration of the incident wavelet. In this paper, $t_d = 2{\cdot}0$ is used. The fluid is assumed to be irrotational, inviscid and acoustic. It is of interest to find the wave field in the composite laminate.

3. FORMULATION

3.1. WAVE FIELD IN LAMINATE

The differential equation governing the elastodynamic behavior of an anisotropic medium in the absence of body force can be written as [22]

$$\rho\ddot{\mathbf{U}} - \mathbf{L}^{\mathrm{T}}\mathbf{c}\mathbf{L}\mathbf{U} = 0, \tag{3}$$

where ρ is the mass density of the material, $\mathbf{U} = [u\ \ v\ \ w]^{\mathrm{T}}$ are the displacement components in the x, y and z directions, respectively, $\mathbf{c}$ is the matrix of elastic constants for the anisotropic material, the dot denotes differentiation with respect to time, $\mathbf{L}$ is the operator matrix given in reference [22] and the superscript T indicates the transposed matrix.

The stresses on a plane $z =$ constant can be expressed in terms of $\mathbf{U}$ as

$$\sigma = \mathbf{L}_z^{\mathrm{T}}\mathbf{c}\mathbf{L}\mathbf{U}, \tag{4}$$

where $\sigma = [\sigma_{xz} \ \sigma_{yz} \ \sigma_{zz}]^{\mathrm{T}}$ is the vector of stresses and the operator matrix $\mathbf{L}_z$ is given in reference [22].

Equation (3) can be solved by a Fourier transform technique. To this end, the following Fourier transform of the displacement with respect to the horizontal co-ordinate x is introduced:

$$\tilde{\mathbf{U}}(z, k) = \int_{-\infty}^{+\infty} \mathbf{U}(z, x) \mathrm{e}^{\mathrm{i}kx} \, \mathrm{d}x, \tag{5}$$

where k is the wave number in the x direction. Application of the Fourier transform to Equations (3) and (4) leads to the equation of motion and stresses in the wave number domain:

$$\rho \ddot{\tilde{\mathbf{U}}} + k^2 \mathbf{D}_{\mathbf{xx}} \tilde{\mathbf{U}} + \mathrm{i}2k \mathbf{D}_{\mathbf{xz}} \frac{\partial \tilde{\mathbf{U}}}{\partial z} - \mathbf{D}_{\mathbf{zz}} \frac{\partial^2 \tilde{\mathbf{U}}}{\partial z^2} = 0, \tag{6}$$

$$\tilde{\sigma} = \mathbf{L}_z^{\mathrm{T}} \mathbf{c} \mathbf{L} \tilde{\mathbf{U}}, \tag{7}$$

where $\mathbf{D}_{xx}$, $\mathbf{D}_{xz}$ and $\mathbf{D}_{zz}$ can be found in reference [23].

The solution of equation (6) follows from Liu *et al.* [23] as

$$\tilde{\mathbf{U}} = \sum_{j=1}^{3} C_j^+ d_j^+ \exp(\mathrm{i}\varsigma_j^+ z) + \sum_{j=1}^{3} C_j^- d_j^- \exp[\mathrm{i}\varsigma_j^- (z - h)], \tag{8}$$

where C_j are constants to be determined using the boundary conditions, d_j is the amplitude, ς_j is the wave number in the z direction, h is the thickness of the layer, the superscripts $+$ and $-$, respectively, denote the variables corresponding to three eigenvalues which are related to wave modes propagating in positive and negative z directions. Note that the term $\mathrm{e}^{-\mathrm{i}\omega t}$ is omitted.

Equation (8) can be rewritten in the matrix form as

$$\tilde{\mathbf{U}} = [\mathbf{V}^+ \mathbf{E}^+ \quad \mathbf{V}^- \mathbf{E}^-] \begin{Bmatrix} \mathbf{C}^+ \\ \mathbf{C}^- \end{Bmatrix}, \tag{9}$$

where $\mathbf{V}^+$, $\mathbf{V}^-$, $\mathbf{E}^+$, $\mathbf{E}^-$, $\mathbf{C}^+$ and $\mathbf{C}^-$ are given by Liu *et al.* [23].

In view of equation (8), the stresses can also be written in the matrix form as

$$\tilde{\sigma} = [\mathbf{P}^+ \mathbf{E}^+ \quad \mathbf{P}^- \mathbf{E}^-] \begin{Bmatrix} \mathbf{C}^+ \\ \mathbf{C}^- \end{Bmatrix}, \tag{10}$$

where $\mathbf{P}^+$ and $\mathbf{P}^-$ are also given by Liu *et al.* [23].

3.2. WAVE FIELD IN WATER

The governing equation of the fluid can be expressed as

$$\ddot{\Phi} - c_w^2 \left(\frac{\partial^2 \Phi}{\partial x^2} + \frac{\partial^2 \Phi}{\partial z^2} \right) = 0, \tag{11}$$

where Φ is the velocity potential, c_w is the sound velocity in water, and the subscript w stands for water. The pressure p and velocity v_z of water can be given by

$$p = \rho_w \frac{\partial \Phi}{\partial t}, \qquad v_z = -\frac{\partial \Phi}{\partial z}, \tag{12, 13}$$

where ρ_w is the density of water. By the application of the inverse Fourier transform technique, the velocity potential $\tilde{\Phi}$ in the wave number domain can be obtained following the procedure of Liu *et al.* [7] as

$$\tilde{\Phi} = \Psi^+ \exp(\mathrm{i}\varsigma_w^+ z) + \Psi^- \exp(\mathrm{i}\varsigma_w^- z), \tag{14}$$

where

$$\varsigma = \begin{cases} \varsigma_w^+ = \begin{cases} \sqrt{k_w^2 - k^2}, & |k| \leqslant |k_w|, \\ \mathrm{i}\sqrt{k^2 - k_w^2}, & |k| > |k_w|, \end{cases} \\ \varsigma_w^- = \begin{cases} -\sqrt{k_w^2 - k^2}, & |k| \leqslant |k_w|, \\ -\mathrm{i}\sqrt{k^2 - k_w^2}, & |k| > |k_w|, \end{cases} \end{cases} \tag{15}$$

where $k_w = \omega/c_w$, $|k|$ and $|k_w|$ are the absolute values of k and k_w, respectively, and the constants Ψ^+ and Ψ^- can be determined by boundary conditions. The first term on the right-hand side of equation (14) is related to the wave mode propagating in the positive z-direction and the second term is related to the wave mode propagating in the negative z direction.

The water depth is assumed to be much larger than the plate thickness so that the fluid domains can be treated as infinity and non-reflection boundary conditions are applicable on the top surface of the fluid above the plate and the bottom surface of the fluid below the plate. For the top part of water, the second term in the expression of the velocity potential has to be zero to satisfy the non-reflection boundary conditions. Thus, we have

$$\tilde{\Phi}_{T\alpha} = \Psi_{T\alpha}^+ \exp(\mathrm{i}\varsigma_\alpha z) \quad \text{for } |k| \leqslant |k_w|, \tag{16}$$

where $\varsigma_\alpha = \sqrt{k_w^2 - k^2}$, the subscript T stands for the top part of water and

$$\tilde{\Phi}_{T\beta} = \Psi_{T\beta}^+ \exp(-\varsigma_\beta z) \quad \text{for } |k| > |k_w|, \tag{17}$$

where $\varsigma_\beta = \sqrt{k^2 - k_w^2}$. For the bottom part of water, the first term in the expression of the velocity potential has to be zero; hence,

$$\tilde{\Phi}_{B\alpha} = \Psi_{B\alpha}^- \exp(-\mathrm{i}\varsigma_\alpha z) \quad \text{for } |k| \leqslant |k_w|, \tag{18}$$

$$\tilde{\Phi}_{B\beta} = \Psi_{B\beta}^- \exp[\varsigma_\beta (z - H_w)] \quad \text{for } |k| > |k_w|, \tag{19}$$

where the subscript B stands for the bottom part of water. Substituting equations (16)–(19) into equations (12) and (13), we have

$$\tilde{p}_{T\alpha} = -\mathrm{i}\omega\rho_w \Psi_{T\alpha}^+ \exp(\mathrm{i}\varsigma_\alpha z), \qquad \tilde{p}_{T\beta} = -\mathrm{i}\omega\rho_w \Psi_{T\beta}^+ \exp(-\varsigma_\beta z), \tag{20, 21}$$

$$\tilde{v}_{zT\alpha} = -\mathrm{i}\varsigma_\alpha \Psi_{T\alpha}^+ \exp(\mathrm{i}\varsigma_\alpha z), \qquad \tilde{v}_{zT\beta} = \varsigma_\beta \Psi_{T\beta}^+ \exp(-\varsigma_\beta z) \tag{22, 23}$$

for the top part of water and

$$\tilde{p}_{B\alpha} = -\mathrm{i}\omega\rho_w \Psi^-_{T\alpha} \exp(-\mathrm{i}\varsigma_\alpha z), \qquad \tilde{p}_{B\beta} = -\mathrm{i}\omega\rho_w \Psi^-_{B\beta} \exp(\varsigma_\beta (z - H_w)), \tag{24, 25}$$

$$\tilde{v}_{zB\alpha} = \mathrm{i}\varsigma_\alpha \Psi^-_{B\alpha} \exp(-\mathrm{i}\varsigma_\alpha z), \qquad \tilde{v}_{zB\beta} = -\varsigma_\beta \Psi^-_{B\beta} \exp(\varsigma_\beta (z - H_w)) \tag{26, 27}$$

for the bottom part of water.

The expressions for the pressure and velocity of the top and bottom parts of water are obtained in terms of wave modes with unknown constants respectively. These constants will be determined using boundary conditions in the next section.

3.3. BOUNDARY CONDITIONS

In a laminate code, a lamina numbering goes from the bottom to the top surface. The boundary condition on the bottom water–plate interface is

$$-(\tilde{\sigma}_{zz})^L_1 = \tilde{p}_B|_{z=0} \tag{28}$$

where the subscript 1 stands for the 1st layer, and the superscript L denotes the lower surface of the layer. The boundary conditions on the interfaces between plies are

$$\begin{matrix} \tilde{\sigma}^U_n - \tilde{\sigma}^L_{n+1} = 0 \\ \tilde{\mathbf{U}}^U_n = \tilde{\mathbf{U}}^L_{n+1} \end{matrix} \quad \text{for } 1 < n < N-1, \tag{29}$$

where the subscripts n and $n+1$ denote the layer numbers, and the superscript U denotes the upper surface of the layer. On the top water–plate interface, the boundary condition is given by

$$(\tilde{\sigma}_{zz})^U_N - \tilde{p}_T|_{z=0} = \tilde{F}, \tag{30}$$

where the subscript N stands for the Nth layer of the plate, and $\tilde{F}$ is the Fourier transform of F.

It follows from equations (20), (21), (24) and (25) that the pressure of water at the top water–plate interface and the bottom water–plate interface are, respectively,

$$\tilde{p}_{T\alpha}|_{z=0} = -\mathrm{i}\omega\rho_w \Psi^+_{T\alpha}, \qquad \tilde{p}_{T\beta}|_{z=0} = -\mathrm{i}\omega\rho_w \Psi^+_{T\beta}, \tag{31, 32}$$

$$\tilde{p}_{B\alpha}|_{z=0} = -\mathrm{i}\omega\rho_w \Psi^-_{B\alpha}, \qquad \tilde{p}_{B\beta}|_{z=0} = -\mathrm{i}\omega\rho_w \Psi^-_{B\beta}, \tag{33, 34}$$

The velocities of water at the top water–plate interface and the bottom water–plate interface can be obtained from equations (22), (23), (26) and (27):

$$\tilde{v}_{zT\alpha}|_{z=0} = -\mathrm{i}\varsigma_\alpha \Psi^+_{T\alpha}, \qquad \tilde{v}_{zT\beta}|_{z=0} = \varsigma_\beta \Psi^+_{T\beta}, \tag{35, 36}$$

$$\tilde{v}_{zB\alpha}|_{z=0} = \mathrm{i}\varsigma_\alpha \Psi^-_{B\alpha}, \qquad \tilde{v}_{zB\beta}|_{z=0} = -\varsigma_\beta \Psi^-_{B\beta}. \tag{37, 38}$$

Using the displacement continuity condition of the plate and water at the two water–plate interfaces, the velocities of water at the two surfaces of the plate can also be expressed in terms of the plate displacement as

$$\tilde{v}_{zT}|_{z=0} = \frac{\partial \tilde{w}_N}{\partial t}, \qquad \tilde{v}_{zB}|_{z=0} = \frac{\partial \tilde{w}_1}{\partial t}. \tag{39, 40}$$

In equations (39) and (40), $\tilde{w}_N = \mathbf{n}\tilde{\mathbf{U}}_N$ and $\tilde{w}_1 = \mathbf{n}\tilde{\mathbf{U}}_1$ are the upper and lower surface displacements in the z direction and $\mathbf{n} = [0\ 0\ 1]$. Substituting equation (9) into equations (39) and (40) results in

$$\tilde{v}_{zT}|_{z=0} = -\mathrm{i}\omega\mathbf{n}[\mathbf{V}_N^+\,\mathbf{E}_{hN}^+\ \mathbf{V}_N^-]\begin{Bmatrix}\mathbf{C}_N^+\\ \mathbf{C}_N^-\end{Bmatrix}, \tag{41}$$

$$\tilde{v}_{zB}|_{z=0} = -\mathrm{i}\omega\mathbf{n}[-\mathbf{V}_1^+ \quad -\mathbf{V}_1^-\,\mathbf{E}_1^-]\begin{Bmatrix}\mathbf{C}_1^+\\ \mathbf{C}_1^-\end{Bmatrix}. \tag{42}$$

For the top part of water, comparing equations (35) and (36) with equation (41) yields

$$\Psi_{T\alpha}^+ = \frac{\omega}{\varsigma_\alpha}\mathbf{n}[\mathbf{V}_N^+\,\mathbf{E}_{hN}^+\ \mathbf{V}_N^-]\begin{Bmatrix}\mathbf{C}_N^+\\ \mathbf{C}_N^-\end{Bmatrix}, \tag{43}$$

$$\Psi_{T\beta}^+ = -\frac{\mathrm{i}\omega}{\varsigma_\beta}\mathbf{n}[\mathbf{V}_N^+\,\mathbf{E}_{hN}^+\ \mathbf{V}_N^-]\begin{Bmatrix}\mathbf{C}_N^+\\ \mathbf{C}_N^-\end{Bmatrix}. \tag{44}$$

For the bottom part of water, comparing equations (37) and (38) with equation (42) leads to

$$\Psi_{B\alpha}^- = -\frac{\omega}{\varsigma_\alpha}\mathbf{n}[-\mathbf{V}_1^+ \quad -\mathbf{V}_1^-\,\mathbf{E}_{h1}^-]\begin{Bmatrix}\mathbf{C}_1^+\\ \mathbf{C}_1^-\end{Bmatrix}, \tag{45}$$

$$\Psi_{B\beta}^- = \frac{\mathrm{i}\omega}{\varsigma_\beta}\mathbf{n}[-\mathbf{V}_1^+ \quad -\mathbf{V}_1^-\,\mathbf{E}_{h1}^-]\begin{Bmatrix}\mathbf{C}_1^+\\ \mathbf{C}_1^-\end{Bmatrix}. \tag{46}$$

Substituting equations (43)–(46) into equations (31)–(34) yields

$$\tilde{p}_{T\alpha}|_{z=0} = -\frac{\mathrm{i}\omega^2\rho_w}{\varsigma_\alpha}\mathbf{n}[\mathbf{V}_N^+\,\mathbf{E}_{hN}^+\ \mathbf{V}_N^-]\begin{Bmatrix}\mathbf{C}_N^+\\ \mathbf{C}_N^-\end{Bmatrix}, \tag{47}$$

$$\tilde{p}_{T\beta}|_{z=0} = -\frac{\omega^2\rho_w}{\varsigma_\beta}\mathbf{n}[\mathbf{V}_N^+\,\mathbf{E}_{hN}^+\ \mathbf{V}_N^-]\begin{Bmatrix}\mathbf{C}_N^+\\ \mathbf{C}_N^-\end{Bmatrix}, \tag{48}$$

$$\tilde{p}_{B\alpha}|_{z=0} = \frac{\mathrm{i}\omega^2\rho_w}{\varsigma_\alpha}\mathbf{n}[-\mathbf{V}_1^+\ \ \mathbf{V}_1^-\,\mathbf{E}_{h1}^-]\begin{Bmatrix}\mathbf{C}_1^+\\ \mathbf{C}_1^-\end{Bmatrix}, \tag{49}$$

$$\tilde{p}_{B\beta}|_{z=0} = \frac{\omega^2 \rho_w}{\varsigma_\beta} \mathbf{n}[-\mathbf{V}_1^+ \quad \mathbf{V}_1^- \mathbf{E}_{h1}^-] \begin{Bmatrix} \mathbf{C}_1^+ \\ \mathbf{C}_1^- \end{Bmatrix}. \tag{50}$$

Consider the boundary condition at the top surface of the plate. Substituting equations (47) and (48) into equation (30) leads to

$$\tilde{F} = \mathbf{n} \begin{bmatrix} \mathbf{P}_N^+ + \dfrac{\mathrm{i}\omega^2 \rho_w}{\varsigma_\alpha} \mathbf{V}_N^+ \mathbf{E}_{hN}^+ & \mathbf{P}_N^- + \dfrac{\mathrm{i}\omega^2 \rho_w}{\varsigma_\alpha} \mathbf{V}_N^- \end{bmatrix} \begin{Bmatrix} \mathbf{C}_N^+ \\ \mathbf{C}_N^- \end{Bmatrix} \tag{51}$$

for $|k| \leqslant |k_w|$ and

$$\tilde{F} = \mathbf{n} \begin{bmatrix} \mathbf{P}_N^+ + \dfrac{\omega^2 \rho_w}{\varsigma_\beta} \mathbf{V}_N^+ \mathbf{E}_{hN}^+ & \mathbf{P}_N^- + \dfrac{\omega^2 \rho_w}{\varsigma_\beta} \mathbf{V}_N^- \end{bmatrix} \begin{Bmatrix} \mathbf{C}_N^+ \\ \mathbf{C}_N^- \end{Bmatrix} \tag{52}$$

for $|k| > |k_w|$, where equation (10) has been used. Consider the boundary condition at the bottom surface of the plate. Substituting equations (49) and (50) equation (28) leads to

$$\mathbf{n} \begin{bmatrix} -\mathbf{P}_1^+ - \dfrac{\mathrm{i}\omega^2 \rho_w}{\varsigma_\alpha} \mathbf{V}_1^+ & -\mathbf{P}_1^- - \dfrac{\mathrm{i}\omega^2 \rho_w}{\varsigma_\alpha} \mathbf{V}_1^- \mathbf{E}_{h1}^- \end{bmatrix} \begin{Bmatrix} \mathbf{C}_1^+ \\ \mathbf{C}_1^- \end{Bmatrix} = 0 \tag{53}$$

for $|k| \leqslant |k_w|$ and

$$\mathbf{n} \begin{bmatrix} -\mathbf{P}_1^+ - \dfrac{\omega^2 \rho_w}{\varsigma_\beta} \mathbf{V}_1^+ & -\mathbf{P}_1^- - \dfrac{\omega^2 \rho_w}{\varsigma_\beta} \mathbf{V}_1^- \mathbf{E}_{h1}^- \end{bmatrix} \begin{Bmatrix} \mathbf{C}_1^+ \\ \mathbf{C}_1^- \end{Bmatrix} = 0 \tag{54}$$

for $|k| > |k_w|$, where equation (10) has been used. Combining equations (51)–(54) and (29) gives

$$\mathbf{AC} = \mathbf{T}, \tag{55}$$

where $\mathbf{T}$ is the vector of tractions acting on the two surfaces and $(N-1)$ interfaces between layers given by

$$\mathbf{T} = [0 \;\; 0 \ldots 0 \;\; \tilde{F}]^{\mathrm{T}}. \tag{56}$$

$\mathbf{C}$ is the constant vector given by

$$\mathbf{C} = [C_1^+ \;\; C_1^- \;\; C_2^+ \;\; C_2^- \;\; \cdots \;\; \cdots \;\; C_N^+ \;\; C_N^-]^{\mathrm{T}} \tag{57}$$

and

$$\mathbf{A} = \begin{bmatrix} -\mathbf{P}_{w1}^{+} & -\mathbf{P}_{w1}^{-}\mathbf{E}_{h1}^{-} & 0 & 0 & 0 & 0 & 0 & \cdots & 0 \\ \mathbf{V}_1^{+}\mathbf{E}_{h1}^{+} & \mathbf{V}_1^{-} & -\mathbf{V}_2^{+} & -\mathbf{V}_2^{-}\mathbf{E}_{h2}^{-} & 0 & 0 & 0 & \cdots & 0 \\ \mathbf{P}_1^{+}\mathbf{E}_{h1}^{-} & \mathbf{P}_1^{-} & -\mathbf{P}_2^{+} & -\mathbf{P}_2^{-}\mathbf{E}_{h2}^{-} & 0 & 0 & 0 & \cdots & 0 \\ 0 & 0 & \mathbf{V}_2^{+}\mathbf{E}_{h2}^{+} & \mathbf{V}_2^{-} & -\mathbf{V}_3^{+} & -\mathbf{V}_3^{-}\mathbf{E}_{h3}^{-} & 0 & \cdots & 0 \\ 0 & 0 & \mathbf{P}_2^{+}\mathbf{E}_{h2}^{+} & \mathbf{P}_2^{+} & -\mathbf{P}_3^{+} & -\mathbf{P}_3^{-}\mathbf{E}_{h3}^{-} & 0 & \cdots & 0 \\ \cdot & \cdot & \cdots & \cdot & \cdot & \cdot & \cdot & \cdots & \cdot \\ \cdot & \cdot & \cdots & \cdot & \cdot & \cdot & \cdot & \cdots & \cdot \\ \cdot & \cdot & \cdots & \cdot & \cdot & \cdot & \cdot & \cdots & \cdot \\ 0 & 0 & \cdots & 0 & 0 & 0 & 0 & \mathbf{P}_{wN}^{+}\mathbf{E}_{hN}^{+} & \mathbf{P}_{wN}^{-} \end{bmatrix}. \tag{58}$$

In equation (58), $\mathbf{P}_n^{+}$, $\mathbf{P}_n^{-}$, $\mathbf{E}_{hn}^{-}$ and $\mathbf{E}_{hn}^{-}$ are given by Liu *et al.* [23] and the 3rd row of matrices $\mathbf{P}_{w1}^{+}$, $\mathbf{P}_{w1}^{-}$ and $\mathbf{P}_{wN}^{+}$, $\mathbf{P}_{wN}^{-}$ are, respectively, given by

$$\mathbf{P}_{w1}^{+} = \mathbf{n}\left(\mathbf{P}_1^{+} + \frac{\mathrm{i}\omega^2\rho_w}{\varsigma_\alpha}\mathbf{V}_1^{+}\right), \qquad \mathbf{P}_{w1}^{-} = \mathbf{n}\left(\mathbf{P}_1^{-} + \frac{\mathrm{i}\omega^2\rho_w}{\varsigma_\alpha}\mathbf{V}_1^{-}\right), \tag{59}$$

$$\mathbf{P}_{wN}^{+} = \mathbf{n}\left(\mathbf{P}_N^{+} + \frac{\mathrm{i}\omega^2\rho_w}{\varsigma_\alpha}\mathbf{V}_N^{+}\right), \qquad \mathbf{P}_{wN}^{-} = \mathbf{n}\left(\mathbf{P}_N^{-} + \frac{\mathrm{i}\omega^2\rho_w}{\varsigma_\alpha}\mathbf{V}_N^{-}\right), \tag{60}$$

for $|k| \leqslant |k_w|$ and

$$\mathbf{P}_{w1}^{+} = \mathbf{n}\left(\mathbf{P}_1^{+} + \frac{\omega^2\rho_w}{\varsigma_\beta}\mathbf{V}_1^{+}\right), \qquad \mathbf{P}_{w1}^{-} = \mathbf{n}\left(\mathbf{P}_1^{-} + \frac{\omega^2\rho_w}{\varsigma_\beta}\mathbf{V}_1^{-}\right), \tag{61}$$

$$\mathbf{P}_{wN}^{+} = \mathbf{n}\left(\mathbf{P}_N^{+} + \frac{\omega^2\rho_w}{\varsigma_\beta}\mathbf{V}_N^{+}\right), \qquad \mathbf{P}_{wN}^{-} = \mathbf{n}\left(\mathbf{P}_N^{-} + \frac{\omega^2\rho_w}{\varsigma_\beta}\mathbf{V}_N^{-}\right), \tag{62}$$

for $|k| > |k_w|$.

From equation (55), the constant vector $\mathbf{C}$ can be solved. Then the displacements and stresses in the wave-number domain can be, respectively, calculated from equations (9) and (10). Finally, applying the inverse Fourier transform, the displacement in the spatial domain can be obtained as

$$\mathbf{U}(z, x) = \frac{1}{2\pi}\int_{-\infty}^{\infty} \tilde{\mathbf{U}}(z, k)\tilde{F}(k)\exp(-\mathrm{i}kx)\mathrm{d}k. \tag{63}$$

The integration in equation (63) can be carried out in $(-\infty, -k_A)$, $(-k_A, k_A)$ and $(k_A, +\infty)$, where k_A is a positive value which is large enough so that all the real value poles are located between $-k_A$ and k_A. The first and last semi-infinites can be evaluated by

a scheme given by Xu and Mal [24]. The essential point is to evaluate the second finite integral. If the integrals are evaluated by ordinary routines using equally spaced sampling points [25], the number of sampling points will be large. Especially for large frequency ω, the integrand in equation (63) varies quite rapidly near the pole. Moreover, it is not easy to control the integral accuracy in using equally spaced routines. In view of the considerations, a new quadrature scheme introduced by Liu *et al.* [23] is employed here.

The integrand in equation (63) has poles on the integration axis. This makes the integration along the integration axis more difficult. Complex paths methods for overcoming the difficulties have been introduced by Liu *et al.* [7]. It should be noted that when the fluid effect is considered, complex paths must be used even if the material of a laminate is dissipative. Because the locations of the poles associated with the fluid are independent of the material dissipation of the laminate, introducing material dissipation cannot move the poles off the integration axis. Besides, in the application of the complex path techniques, it should firstly be noticed that the triangular portion in the complex path has to be long enough to get around all the poles associated with the laminate and water. The complex paths should be very close to the real wave number axis to ensure that no poles are included in the triangular loop enclosed by the complex path and real k-axis. $k_{hw} = \pm 0{\cdot}2$ are recommended here.

3.4. WAVE FIELD IN LAMINATES IN TIME DOMAIN

Once the displacement in the frequency domain is obtained, the displacement in the time domain can be calculated by application of the Fourier superposition

$$u_t(t) = \frac{1}{2\pi} \int_{-\infty}^{\infty} U(\omega)\hat{F}(\omega)\exp(\mathrm{i}\omega t)\,\mathrm{d}\omega, \tag{64}$$

where the subscript t indicates the variable in the time domain, and $U(\omega)$ is the response in the frequency domain which can be obtained from equation (63). $\hat{F}(\omega)$ is the Fourier transform of the time dependence of the external force given by

$$\hat{F}(\omega) = \int_{0}^{\infty} F(t)\exp(-\mathrm{i}\omega t)\,\mathrm{d}t. \tag{65}$$

From equation (65), we have

$$\hat{F}(-\omega) = \hat{F}^*(\omega), \tag{66}$$

where the asterisk denotes the complex conjugate. The results in equation (65) are demonstrated in Figure 2(a). Furthermore, from the spectrum of the incident wavelet, the amplitudes become very small when the dimensionless frequencies $\bar{\omega} > 20{\cdot}0$. Hence, the contribution from frequencies higher than 20·0 can be ignored. In the computation in this paper, $0 \leqslant \bar{\omega} \leqslant 20$ is used. In Figure 2(b), the distribution of $U(\omega)$ on the upper surface of a $[C90/G + 45/G - 45]_s$ plate is depicted. Obviously, we have

$$U(-\omega) = U^*(\omega). \tag{67}$$

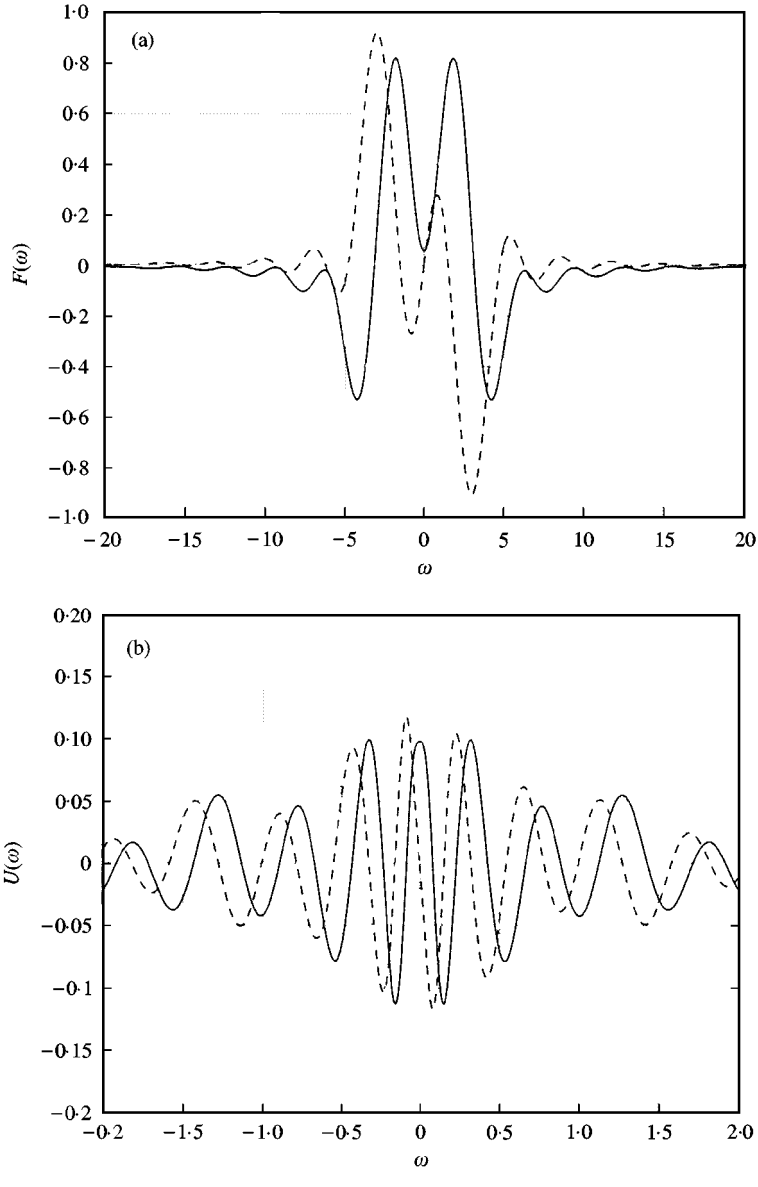

Figure 2. (a) Frequency spectrum of external loading wavelet. (b) Dimensionless displacement in frequency domain on the upper surface of a $[C90/G + 45/G - 45]_s$ plate subjected to a line load. —— $\mathrm{Re}[w(k)]$; – – – $\mathrm{Im}[w(k)]$.

With the help of equations (66) and (67), equation (64) can be simplified as

$$u_t(t) = \frac{1}{\pi}\left[\int_0^\infty (U_R \hat{F}_R - U_1 \hat{F}_1)\cos \omega t \, \mathrm{d}\omega - \int_0^\infty (U_R \hat{F}_1 + U_1 \hat{F}_R)\sin \omega t \, \mathrm{d}\omega, \right. \tag{68}$$

where U_R and U_I are the real and imaginary parts of U respectively; $\hat{F}_R$ and $\hat{F}_I$ are, respectively the real and imaginary parts of $\hat{F}$.

In equation (64), there are singularities of $U(\omega)$ at $\omega = 0$ and cut-off frequencies ($k = 0$). To overcome these difficulties an exponential window method [26, 27] is employed. Instead of equation (64), the displacement in the time domain can be solved by

$$u_t(t) = \frac{e^{\eta t}}{2\pi} \int_{-\infty}^{\infty} U_\omega(\omega - i\eta)\hat{F}_\omega(\omega - i\eta)\exp(-i\omega t)\,d\omega, \tag{69}$$

where η is a small positive value and

$$\hat{F}_\omega(\omega - i\eta) = \int_0^{t_d} e^{-\eta t} F(t)\exp(-i\omega t)\,dt, \tag{70}$$

Since $U_\infty(\omega - i\eta)$ behaves well in $-\infty < \omega < +\infty$, the singularity of U_ω at $\omega = 0$ is avoided.

4. NUMERICAL EXAMPLES

The analysis procedure given above has been incorporated into a FORTRAN code for computing wave propagation in a fluid–plate–fluid system. In this section, numerical results are presented in the form of normal displacements on the upper surface of the plate. Steel and $[C90/G + 45/G - 45]_s$ composite laminated plates are studied. Here, the letters C and G represent carbon/epoxy and glass/epoxy respectively. The numbers following the letters indicate the angle of the fiber orientation with respect to the x-axis. The subscript s denotes that the composite laminate is symmetrically stacked. The material properties of the plates, the density of water and the acoustic wave velocity are given in reference [7]. In all calculations, the following dimensionless parameters are used:

$$\bar{x} = x/H, \quad \bar{u} = c(4,4)u/q_0, \quad \bar{w} = c(4,4)w/q_0, \quad \bar{\omega} = \omega H/c_s,$$

$$\bar{t} = tc_s/H, \quad c_s = \sqrt{c(4,4)/\rho_w}, \quad \bar{c}_w = c_w/c_s, \quad \bar{\rho}_w = \rho_w/\rho_s, \tag{71}$$

where $c(4,4)$ is the reference shear modulus. It is the shear modulus for a steel plate, while it is the on-principal-axis shear modulus in tranversely isotropic plane of the carbon/epoxy for a composite plate.

Two cases are used to verify the program. First of all, we let the density of the bottom part of waer be zero and make a fluid–plate–fluid system become a fluid–plate–free system. In Figure 3(a), responses on the upper surface of a fluid-loaded $[C90/G + 45/G - 45]_s$ plate to a Gaussian beam with $b = 0{\cdot}01$ and $\bar{\omega} = 3{\cdot}14$ are depicted and compared with those from reference [7]. Good agreement is observed. Secondly, we let the densities of the top and bottom parts of waer be zero and make a fluid–plate–fluid system become a dry plate. In Figure 3(b), responses of a $[C90/G + 45/G - 45]_s$ plate to a line load are illustrated and compared with those from reference [23]. Very clearly, they agree very well.

4.1. RESPONSES IN WAVE NUMBER DOMAIN

In Figure 4, the upper surface responses of a completely immersed $[C90/G + 45/G - 45]_s$ composite laminated late to a Gaussian beam with shape factor $b = 0{\cdot}01$ and frequency $\bar{\omega} = 3{\cdot}14$ are presented. The position of observation is at $x/H = 12{\cdot}0$. Figures 4(a) and 4(b)

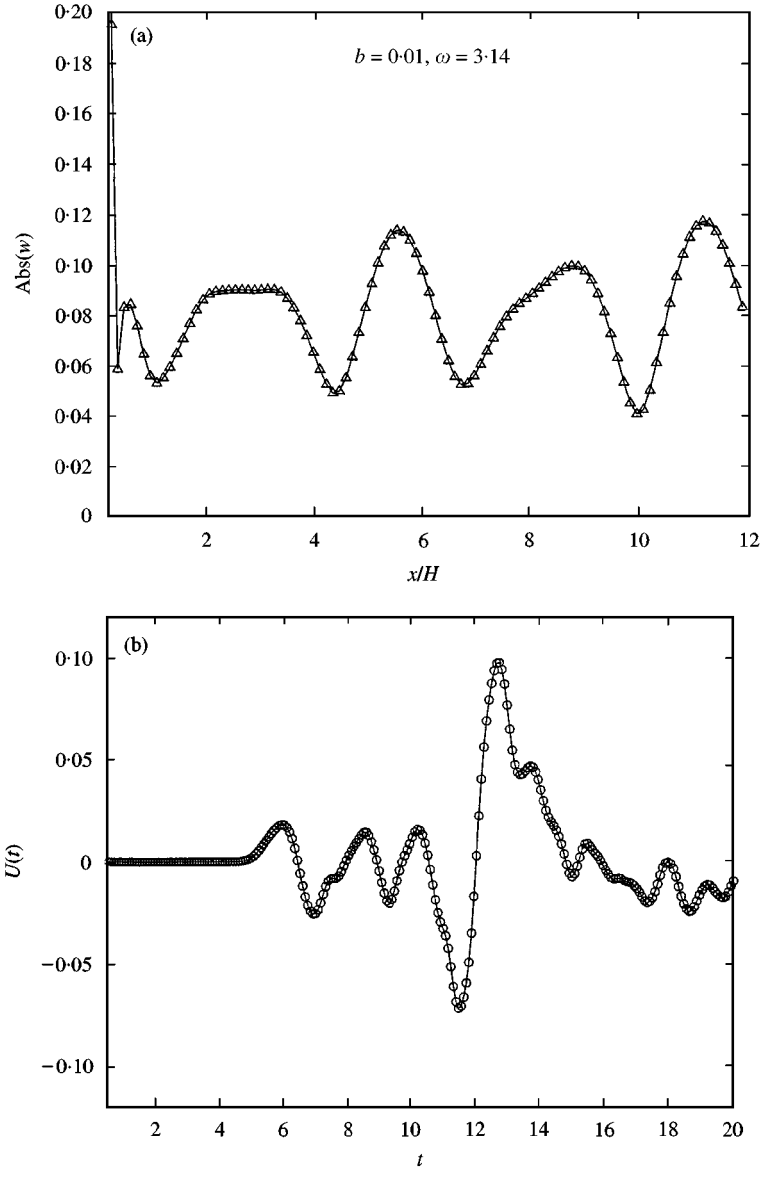

Figure 3. Dimensionless displacement on the upper surface of a $[C90/G + 45/G - 45]_s$ plate. (a) Comparison in frequency domain, —— Liu *et al.* [7]; △ Present analysis. (b) Comparison in time domain, —— Liu *et al.* [7]; ○ Present analysis.

are for the pure elastic laminate and dissipative plates respectively. A comparison of these two figures shows that the material dissipation reduces the magnitudes of the real and imaginary parts of the displacements, but it has little effect on the variation patterns of the real and imaginary parts. In addition, the material dissipation also reverses the peak direction of the imaginary part. In order to discuss the effect of the bottom part of water, the results from Liu *et al.* [7] for a fluid–plate–free system are depicted in these two figures. It can easily be found from these figures that the presence of the bottom part of water reduces the magnitudes of the real and imaginary parts of the surface displacements. The presence of

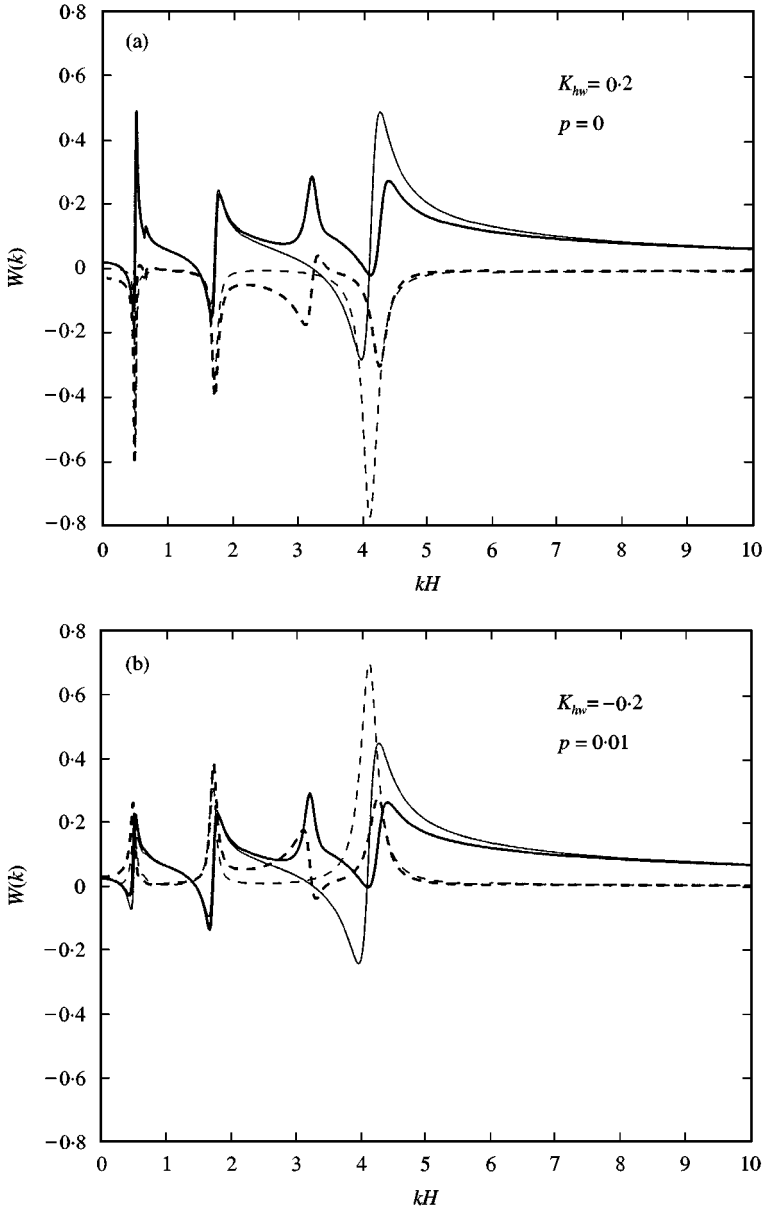

Figure 4. Dimensionless displacement in wave number domain on the upper surface of a $[C90/G + 45/G - 45]_s$ plate subjected to a sharp Gaussian beam pressure with $b = 0{\cdot}01$, $\bar{\omega} = 3{\cdot}14$. Bold lines represent the present analysis, slim lines represent Liu *et al.* [7] (a) Responses of pure elastic plate. (b) Responses of dissipative plate. ——— Re$[w(k)]$; – – – Im$[w(k)]$; —— Re$[w(k)]$; – – – Im$[w(k)]$.

the bottom part of water causes one more peak of the real and imaginary parts. This indicates that the presence of the bottom part of water introduces new poles on the integration axis and changes the variation patterns of the real and imaginary parts.

Next, the effect of frequency is examined. Figure 5 is the same as Figure 4 but $\bar{\omega} = 6{\cdot}28$. The results of the pure elastic and dissipative plates are, respectively, presented in Figures 5(a) and 5(b). Firstly, the findings regarding the material dissipation effect are once again confirmed by comparing these two figures. Secondly, curves in these two figures indicate

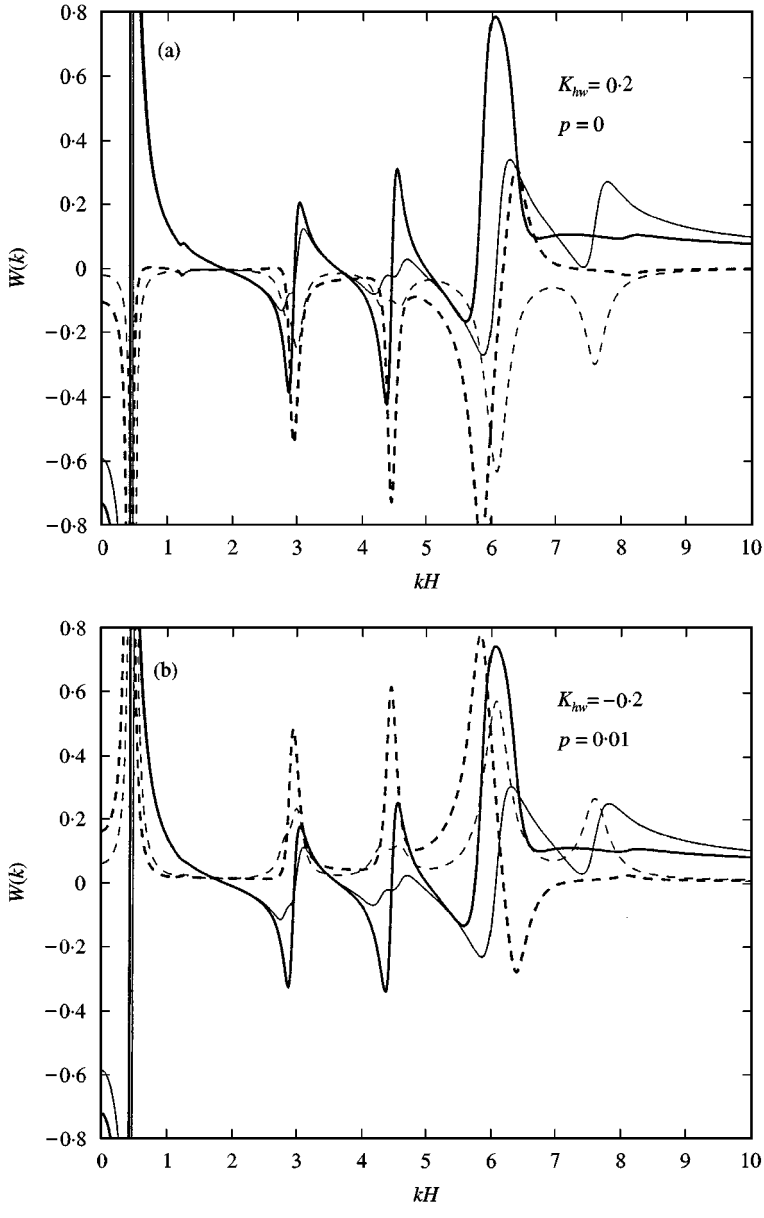

Figure 5. Same as Figure 4, but $\bar{\omega} = 6{\cdot}28$. ——— Re[$w(k)$]; – – – Im[$w(k)$]; —— Re[$w(k)$]; – – – Im[$w(k)$].

that the presence of the bottom part of water not only increases the magnitude of the responses but also alters their distribution. This is contrary to previous findings. It can be concluded that the effect of the bottom part of water is strongly dependent on the frequency of excitation.

4.2. RESPONSES IN FREQUENCY DOMAIN

Figure 6 shows the distribution of the upper surface displacement of a completely submerged steel plate subjected to a Gaussian beam with $b = 0{\cdot}01$. As b is very small, the

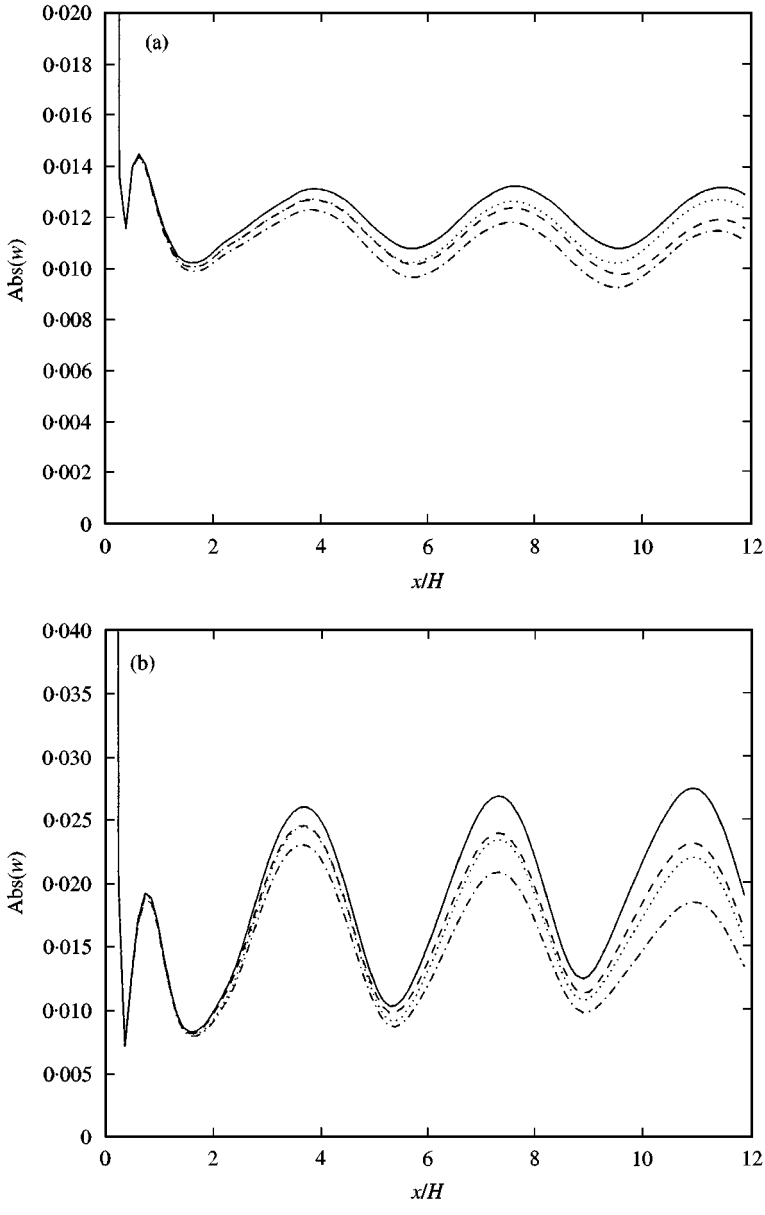

Figure 6. Dimensionless displacements on the upper surface of a steel plate subjected to a Gaussian beam with shape factor $b = 0{\cdot}01$. (a) The Gaussian beam frequency is $\bar{\omega} = 3{\cdot}14$. (b) The Gaussian beam frequency is $\bar{\omega} = 6{\cdot}28$. —— Fluid–plate–free, $p = 0{\cdot}0$; – – – Fluid–plate–free, $p = 0{\cdot}01$; .... Fluid–plate–fluid, $p = 0{\cdot}0$; –·–·– Fluid–plate–fluid, $p = 0{\cdot}01$.

pressure is highly concentrated at the origin. For the sake of comparison, results from Liu *et al.* [7] for the corresponding fluid–plate–free system are also plotted in the same figure. Figures 6(a) and 6(b) are for frequencies 3·14 and 6·28 respectively. Comparing the results of the two systems, the presence of the bottom part of water reduces the amplitude of the responses irrespective of whether the plate is pure elastic or dissipative. The fluid effect becomes stronger as x/H increases. But it should be noted that the presence of water does not alter the distribution pattern of the surface displacement of the steel plate. This is the

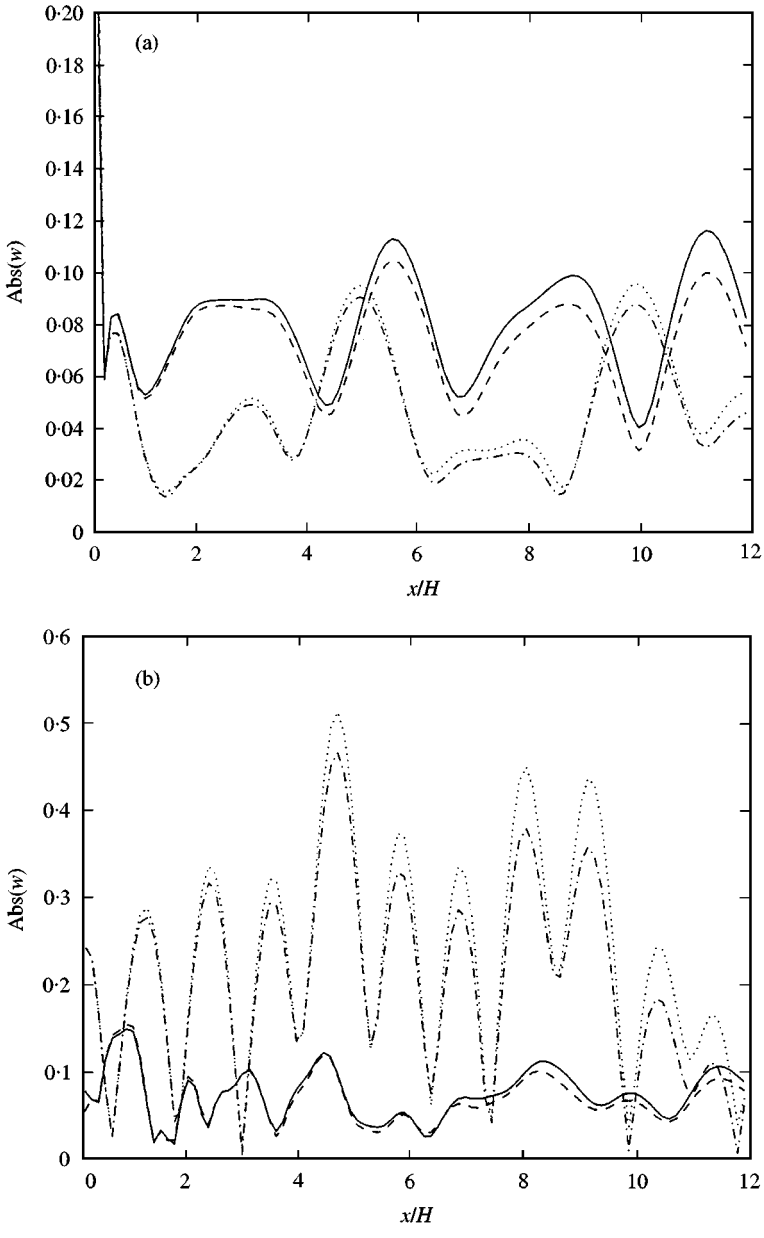

Figure 7. Dimensionless displacements on the upper surface of a $[C90/G + 45/G - 45]_s$ plate subjected to a Gaussian beam with shape factor $b = 0{\cdot}01$. (a) The Gaussian beam frequency is $\bar{\omega} = 3{\cdot}14$. (b) The Gaussian beam frequency is $\bar{\omega} = 6{\cdot}28$. —— Fluid–plate–free, $p = 0{\cdot}0$; – – – Fluid–plate–free, $p = 0{\cdot}01$; .... Fluid–plate–fluid, $p = 0{\cdot}0$; ·–·–·– Fluid–plate–fluid, $p = 0{\cdot}01$.

same as the effect of material dissipation on the surface displacement of the steel plate. That is, the material dissipation does not change the distribution pattern of the surface displacement, but it reduces the magnitude of the surface displacement and the reduction becomes larger with an increase in x/H.

Figure 7 is the same as Figure 6 but for a $[C90/G + 45/G - 45]_s$ composite laminated plate. In order to investigate the effect of the bottom part of water, the results of the corresponding fluid–plate–free system from Liu *et al.* [7] are also plotted in the same plots.

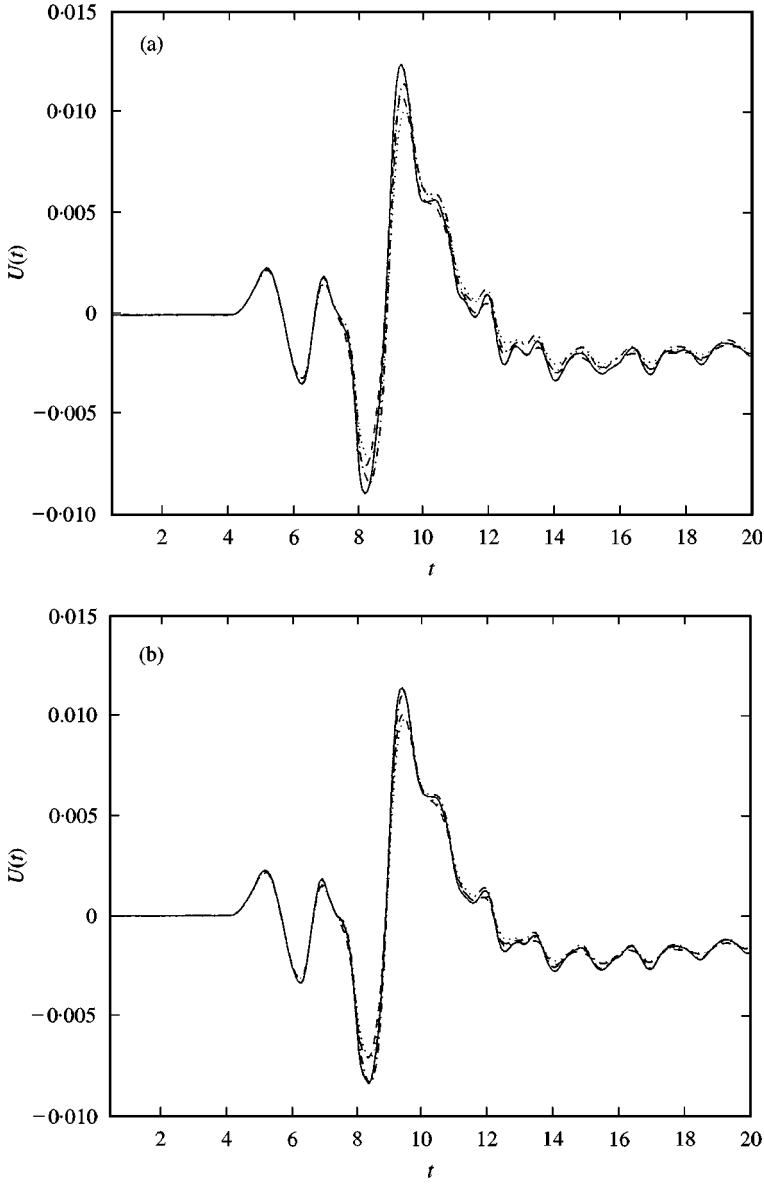

Figure 8. Surface displacement in x direction of a steel plate subjected to a Gaussian beam with shape factor $b = 0{\cdot}01$. (a) Fluid–plate–free system. —— Dry plate, $p = 0$; – – – Dry plate, $p = 0{\cdot}01$; ·–·–·– Fluid-plate-free, $p = 0$; ···· Fluid-plate-free, $p = 0{\cdot}01$. (b) Fluid–plate–fluid system. —— Fluid–plate–free, $p = 0$; – – – Fluid–plate–free, $p = 0{\cdot}01$; ·–·–·– Fluid–plate–fluid, $p = 0$; ···· Fluid–plate–fluid, $p = 0{\cdot}01$.

Once again, the material dissipation effect is confirmed; namely, it can reduce the magnitude of the surface displacement, but does not change the distribution pattern of the surface displacement. When the loading frequency is 3·14, the magnitude of the surface displacement of the fluid–plate–fluid system is smaller than that of the fluid–plate–free system. Besides, the pronounced effect of the bottom part of water shifts the peaks and dips of the surface responses. When the loading frequency changes to 6·28, the magnitude of the surface displacement of the fluid–plate–fluid system is larger than that of the fluid–plate–free system. This phenomenon is similar to the finding for responses in the wave

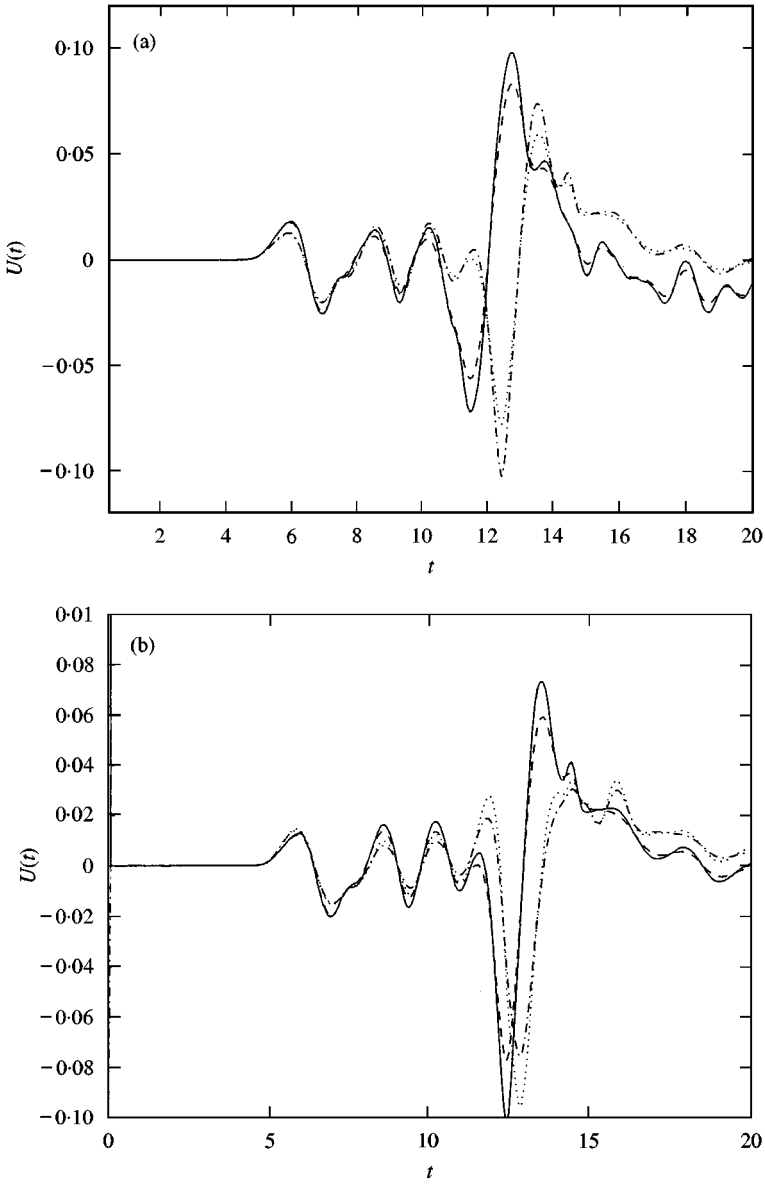

Figure 9. Surface displacement in x direction of a $[C90/G + 45/G - 45]_s$ plate subjected to a Gaussian beam with shape factor $b = 0{\cdot}01$. (a) Fluid–plate–free system. —— Dry plate, $p = 0$; – – – Dry plate, $p = 0{\cdot}01$; ·–·–· Fluid-plate-free, $p = 0$; ···· Fluid-plate-free, $p = 0{\cdot}01$. (b) Fluid–plate–fluid system. —— Fluid–plate–free, $p = 0$; – – – Fluid–plate–free, $p = 0{\cdot}01$; ···· Fluid–plate–fluid, $p = 0$; ·–·–· Fluid–plate–fluid, $p = 0{\cdot}01$.

number domain. A comparison of Figure 7 and Figure 6 shows that water has a greater impact on the composite laminate than on the steel plate. The reason is the lower ratio of the composite to water density. Therefore, the effect of water must be taken into account in the investigation of waves in a fluid-loaded composite laminate.

4.3. RESPONSES IN TIME DOMAIN

Figure 8 shows the surface displacements in the x-direction of a completely immersed steel plate subjected to a Gaussian beam with shape factor $b = 0{\cdot}01$. The observing position

is at $x/H = 12{\cdot}0$. Both the pure elastic and dissipative plates are considered. Figure 8(a) illustrates the effect of the top part of water, while Figure 8(b) illustrates the effect of the bottom part of water. It can be seen from these two figures that the material dissipation and the presence of water all cause a slight decrease in the peak and dip of the displacements, but they seem to have little effect on the variation pattern of the responses.

Figure 9 is the same as Figure 8 but for a $[C90/G + 45/G - 45]_s$ composite laminate. Clearly, the material dissipation affects the surface displacements of the laminate in a similar way that it does the foregoing steel plate. But the effect of water on the surface displacements of the composite laminate should specially be noticed. Firstly, the presence of water not only alters the magnitude of the responses but also causes the displacements to shift along the time t-axis. Also, it gives rise to one more dip and peak occurring just before the maximum dip and peak.

5. CONCLUSIONS

An analytical method has been presented for analyzing the elastodynamic responses of anisotropic laminated plate in contact with water on both sides. The responses of steel and composite laminated plates to a Gaussian beam are investigated in the wave number, frequency and time domains. Complex path techniques, the exponential window method and the effective quadrature scheme are proposed to overcome the difficulties in integration. Based on the numerical results presented in this paper, the following conclusions may be drawn:

(1) The material dissipation reduces the magnitude of the responses and reverses the peak direction of the imaginary part of responses in wave number domain, but has no effects on the variation patterns of the responses.
(2) The presence of water reduces the magnitude of the responses of a steel plate, but it does not alter the distribution of the responses of a steel plate.
(3) The effect of water on the responses of a composite laminated plate is considerable. It not only affects significantly the magnitude of the responses and shifts the peak and dips of the responses, but also changes the distribution of the responses. Also, the effect of water is strongly dependent on the frequency of an incident wave.
(4) Owing to the lower ratio of composite to water density, the fluid effect on the responses of a composite plate is more remarkable than on those of a steel plate. Therefore, the fluid effect must be taken into account in the analyses of wave propagation in a fluid-loaded composite laminate.

REFERENCES

1. G. MOTT 1970 *Journal of the Acoustical Society of America* **50**, Part 2, 819–829. Reflection and refraction coefficients at a fluid–solid interface.
2. E. G. HENNEKE and G. L. JONES 1976 *Journal of the Acoustical Society of America* **59**, 204–205. Critical angle for reflection at a liquid–solid interface in single crystals.
3. Z. ATALAR 1983 *Journal of the Acoustical Society of America* **73**, 435–440. Reflection of ultrasonic waves at a liquid–cubic–liquid interface.
4. O. ARIKAN, E. TELATAR and A. ATALAR 1989 *Journal of the Acoustical Society of America* **85**, 1–10. Reflection coefficient null of acoustic waves at a liquid–anisotropic–solid interface.
5. D. E. CHIMENTI and A. H. NAYFEH 1989 *Journal of the Acoustical Society of America* **85**, 555–560. Ultrasonic leaky waves in a solid plate separating a fluid and vacuum.
6. G. R. LIU, K. Y. LAM and E. S. CHAN 1996 *Shock and Vibration* **3**, 419–433. Stress waves in composite laminates excited by transverse plane shock waves.

7. G. R. LIU, X. J. WANG and Z. C. XI 1999 *International Journal of Mechanical Sciences*. An exact solution for wave propagation in composite laminates submerged in water (submitted).
8. A. H. NAYFEH 1991 *Wave motion* **14**, 55–67. Elastic wave reflection from liquid–anisotropic substrate interfaces.
9. A. H. NAYFEH and T. W. TAYLOR 1988 *Journal of the Acoustical Society of America* **84**, 2187–2191. Surface wave characteristics of fluid-loaded multilayered media.
10. J. QU, J. D. ACHENBACH and R. A. ROBERTS 1989 *IEEE Transactions on Ultrasonics, Ferroelectrics, and Frequency Control* **36**, 2890–286. Reciprocal reflections for transmission coefficients: Theory and application.
11. V. S. AHN and J. D. ACHENBACH 1991 *Ultrasonics* **29**, 482–489. Response of line focus acoustic microscope to specimen containing a subsurface crack.
12. G. R. LIU, J. D. ACHENBACH, J. O. KIM and Z. L. LI 1992 *Journal of the Acoustical Society of America* **92**, 2734–2740. A combined finite element method/boundary element method technique for $V(z)$ curves of anisotropic-layer/substrate configurations.
13. K. MAMPAERT and O. LEROY 1988 *Journal of the Acoustical Society of America* **83**, 1390–1398. Reflection and transmission of normally incident ultrasonic waves on periodic solid–liquid interfaces.
14. T. J. PLONA, K. W. WINKLER and M. SCHOENBERG 1987 *Journal of the Acoustical Society of America* **81**, 1227–1234. Acoustic waves in alternating fluid/solid layers.
15. R. D. FAY and O. V. FORTIER 1951 *Journal of the Acoustical Society of America* **23**, 339–346. Transmission of sound through steel plates immersed in water.
16. A. H. NAYFEH and D. E. CHIMENTI 1988 *Journal of the Acoustical Society of America* **55**, 863–870. Ultrasonic wave reflection from liquid-coupled orthotropic plates with application to fibrous composites.
17. V. DAYAL and V. K. KINRA 1989 *Journal of the Acoustical Society of America* **85**, 2268–2276. Leaky Lamb waves in an anisotropic plate. I: An exact solution and experiments.
18. V. DAYAL and V. K. KINRA 1991 *Journal of the Acoustical Society of America* **89**, Part 1, 1590–1596. Leaky Lamb waves in an anisotropic plate. II: Nondestructive evaluation of matrix cracks in fiber-reinforced composites.
19. A. H. NAYFEH and D. E. CHIMENTI 1991 *Journal of the Acoustical Society of America* **89**, 542–549. Elastic wave propagation in fluid-loaded multiaxial anisotropic media.
20. D. E. CHIMENTI and A. H. NAYFEH 1990 *Journal of the Acoustical Society of America* **87**, 1409–1415. Ultrasonic reflection and guided wave propagation in biaxially laminated composite plates.
21. A. H. NAYFEH and D. E. CHIMENTI 1988 *Journal of the Acoustical Society of America* **83**, 1736–1743. Propagation of guided waves in fluid-coupling plates of fiber-reinforced composite.
22. E. KAUSEL 1986 *International Journal of numerical methods Engineering* **23**, 1567–1578. Wave propagation in anisotropic layered media.
23. G. R. LIU, K. Y. LAM and J. TANI 1995 *Mechanics of Composite Materials and Structures* **2**, 227–241. An exact method for analyzing elastodynamic responses of anisotropic laminates to line loads.
24. P. C. XU and A. K. MAL 1987 *Bulletin of the Seismological Society of America* **77**, 1823–1837. Calculation of the inplane Green's functions for a layered viscoelastic solid.
25. G. R. LIU and J. TANI 1994 *ASME Journal of Vibration and Acoustics* **116**, 440–448. Surface waves in functionally gradient piezoelectric plates.
26. N. VASUDEVAN and A. K. MAL 1985 *ASME Journal of Applied Mechanics* **52**, 356–362. Responses of an elastic plate to localized transient sources.
27. E. KAUDEL and J. M. ROËSSET 1992 *ASCE Journal of Engineering Mechanics* **118**, 721–734. Frequency domain analysis of undamped systems.